GEOLOGICAL JOURNAL
*Geol. J.* **49**: 1–14 (2014)
Published online 7 January 2013 in Wiley Online Library
(wileyonlinelibrary.com). DOI: 10.1002/gj.2481

# Petrogenesis of the Yangchang Mo-bearing granite in the Xilamulun metallogenic belt, NE China: geochemistry, zircon U–Pb ages and Sr–Nd–Pb isotopes

***QINGDONG ZENG*, JINHUI YANG, ZUOLUN ZHANG, JIANMING LIU and XIAOXIA DUAN***

*Key Laboratory of Mineral Resources, Institute of Geology and Geophysics, Chinese Academy of Sciences, PO Box 9825, Beijing 100029, China*

The Yangchang granite-hosted Mo deposit is typical of the Xilamulun metallogenic belt, which is one of the important Mo–Pb–Zn–Ag producers in China. A combination of major and trace element, Sr, Nd and Pb isotope, and zircon U–Pb age data are reported for the Yangchang batholith to constrain its petrogenesis and Mo mineralization. Zircon LA-ICPMS U–Pb dating yields mean ages of $138 \pm 2$ and $132 \pm 2$ Ma for monzogranite and granite porphyry, respectively. The monzogranites and granite porphyries are calc-alkaline with $K_2O/Na_2O$ ratios of 0.75–0.92 and 1.75–4.42, respectively. They are all enriched in large-ion lithophile elements (LILEs) and depleted in high-field-strength elements (HFSEs) with negative Nb and Ta anomalies in primitive-mantle-normalized trace element diagrams. The monzogranites have relatively high Sr (380–499 ppm) and Y (14–18 ppm) concentrations, and the granite porphyries have lower Sr (31–71 ppm) and Y (5–11 ppm) concentrations than those of monzogranites. The monzogranites and granite porphyries have relatively low initial Sr isotope ratios of 0.704573–0.705627 and 0.704281, respectively, and similar $^{206}Pb/^{204}Pb$ ratios of 18.75–18.98 and 18.48–18.71, respectively. In contrast, the $\varepsilon_{Nd}(t)$ value (−3.7) of granite porphyry is lower than those of monzogranites (−1.5 to −2.7) with Nd model ages of about 1.0 Ga. These geochemical features suggest that the monzogranite and granite porphyries were derived from juvenile crustal rocks related to subduction of the Paleo-Pacific plate under east China. 

*Received 28 March 2012; accepted 20 November 2012*

KEY WORDS Yangchang granite; Xilamulun metallogenic belt; U–Pb zircon age; Sr-Nd-Pb isotopes; juvenile crust; subduction of Paleo-Pacific plate

## 1. INTRODUCTION

The Xilamulun metallogenic belt at the northern margin of the North China Craton is an important Mo–Ag–Pb–Zn producer in China (Fig. 1). The Xilamulun metallogenic belt extends E–W for approximately 400 km and N–S for 100 km. It contains medium- to large-scale Mo deposits, such as the Chehugou, Xiaodonggou, Jiguanshan, Nianzigou, Yangchang, Baimashi and Kulitu deposits (Zeng *et al*., 2009, 2011a). Recent studies (Zeng *et al*., 2011a, b) show that the ore-forming epoch in the Xilamulun metallogenic belt includes three stages: Early Triassic, Late Jurassic and Early Cretaceous. The Triassic Mo deposits and granitoids are related to the Paleo-Asian Ocean tectonic evolution. The Late Jurassic Mo deposits and granitoids are related to Paleo-Pacific tectonic evolution, and the Early Cretaceous Mo deposits and granitoids are related to lithosphere thinning in east China (Zeng *et al*., 2011a). Previous studies on the Xilamulun metallogenic belt show that the Mo mineralization is related to the granitoids in genesis (Nie *et al*., 2007; Wu *et al*., 2008, 2011b; Qin *et al*., 2009; Zeng *et al*., 2009, 2010a, 2011b; Zhang *et al*., 2009; Liu *et al*., 2010).

Zeng *et al*. (2010b) reported a Re–Os isochron age of $138.5 \pm 4.5$ Ma for molybdenite from the Yangchang granite-hosted Mo deposit that suggested its mineralization age was Early Cretaceous, and they proposed that the metallogenesis had a genetic relationship with Cretaceous granitic magmatic activity. To further understand the metallogenesis of the Mo deposit and its genetic relationship to the host granitoids, we present the whole-rock elemental geochemistry, Sr–Nd–Pb isotope geochemistry and U–Pb zircon geochronology of the host granitoids for the Yangchang deposit, to constrain the ages and petrogenesis of the host granitoids. We also assess the broader tectonomagmatic implication of the Yangchang Mo deposit and its host granitoids. Our results also have significant implications for constraining the molybdenum resource of the Mo deposit.

## 2. GEOLOGICAL SETTING

The Xilamulun metallogenic belt is divided into two parts by the Xilamulun River Fault: the Late Palaeozoic Accretion

*Correspondence to: Q. Zeng, Key Laboratory of Mineral Resources, Institute of Geology and Geophysics, Chinese Academy of Sciences, PO Box 9825, Beijing 100029, China. E-mail: zengqingdong@mail.iggcas.ac.cn

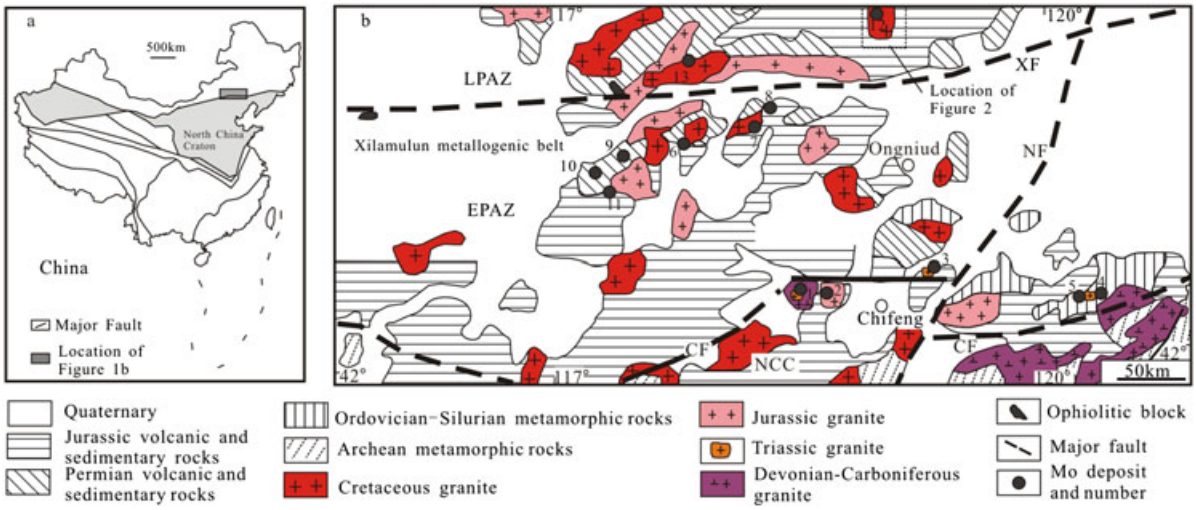


Figure 1. (a) Location map of the Xilamulun metallogenic belt. (b). Geological map of the Xilamulun metallogenic belt in NE China (adapted from Zeng *et al*., 2009). NCC—North China Craton; EPAZ—Early Paleozoic accretion zone; LPAZ—Late Paleozoic accretion zone; XF—Xilamulun River Fault; NF—Neijiang Fault; CF—Chifeng Fault. Molybdenum deposit name: 1—Chehugou; 2—Nianzigou; 3—Jiguanshan; 4—Kulitu; 5—Baimashi; 6—Xiaodonggou; 7—Gangzi; 8—Tuohe; 9—Hongshanzi; 10—Xinfangzi; 11—Talagou; 12—Yangchang; 13—Longtoushan. This figure is available in colour online at wileyonlinelibrary.com/journal/gj

Zone (LPAZ) in the north and the Early Palaeozoic Accretion Zone (EPAZ) in the south (Fig. 1).

The LPAZ is mainly composed of Permian volcanic and sedimentary rocks, and covered by Mesozoic rocks. Permian rocks include (in upward order) (BGMR, 1991): (1) the Lower Permian Qingfengshan Formation, consisting of graywake and siltstone with tuffaceous intercalation, (2) the Lower Permian Dashizhai Formation, consisting of submarine lava and tuff (principally andesitic, and secondly felsic and basaltic) with arenite, characterized by very strong facies change, (3) the Lower Permian Huanggangliang Formation, consisting of mix-bedded sandstone/slate with limestone (now marble or crystalline limestone) and tuffite, and (4) the Upper Permian Linxi Formation, consisting of terrestrial sandstone, siltstone and mudstone with tuffaceous intercalation.

The EPAZ is mainly composed of Ordovician–Silurian metamorphic rocks consisting of biotite plagioclase schist, gneiss, hornblende schist, phyllite and marble, and covered by Permian and Mesozoic rocks. The Permian rocks are divided into two major groups: (i) the Lower Permian units comprising metasandstone, slate, meta-andesite and tuff and (ii) the Upper Permian units comprising marble, metasandstone and meta-andesite. The Mesozoic rocks appear extensively throughout the region and include Jurassic and Cretaceous rocks. The Jurassic rocks are composed of conglomerate, sandstone, shale, andesite, dacite, tuff breccia and tuff with coal layers. The Cretaceous rocks are composed of andesite, dacite, rhyolite, tuff breccia, conglomerate and sandstone with thin coal layers (BGMR, 1991).

In the Yangchang area (Fig. 2a, b), the Lower Permian strata are composed of metamorphic sandstone, siltstone, tuff, slate and marble. The strata are intruded by the Yangchang granitic body and covered by Jurassic rocks (Fig. 2a, b). The Jurassic rocks are widely distributed in the study area and include Middle Jurassic tuff conglomerate and sandstone and Late Jurassic tuff breccia and tuff.

## 3. FIELD RELATIONS AND PETROGRAPHY

Several intrusions and subvolcanic rocks are found in the Xilamulun metallogenic belt, including mainly Triassic–Cretaceous monzogranite, porphyritic granite and syenogranite porphyry (Zeng *et al*., 2011a). The Triassic monzogranite and porphyritic granite develop in Laojiagou, Kulitu, Baimashi and Chehugou deposits. The Triassic monzogranite (LA–ICPMS zircon U–Pb age: 238–241 Ma, Zeng *et al*., 2012) is composed of K-feldspar (25–35%), plagioclase (25–35%), quartz (20–30%) and biotite (<5%). Accessory minerals are zircon, magnetite and apatite. The Triassic porphyritic granite (SHRIMP zircon U–Pb age: 245 Ma, Zeng *et al*., 2011a) is typically porphyritic, with crystals of quartz, plagioclase and K-feldspar, which commonly represent 20% of the rock. The matrix mineral assemblage includes quartz, K-feldspar and plagioclase, with minor biotite. Accessory minerals include magnetite, zircon and apatite. The Triassic intrusions intrude the Permian strata and Devonian granitoids. The Jurassic monzogranite (SHRIMP zircon U–Pb age: 152 Ma, Zeng *et al*., 2011a) is composed of plagioclase (40%), K-feldspar (35%), quartz (25%) and biotite (5%). Accessory minerals are sphene, zircon and magnetite. The Jurassic intrusions intrude the Jurassic volcanics and Permian strata. The

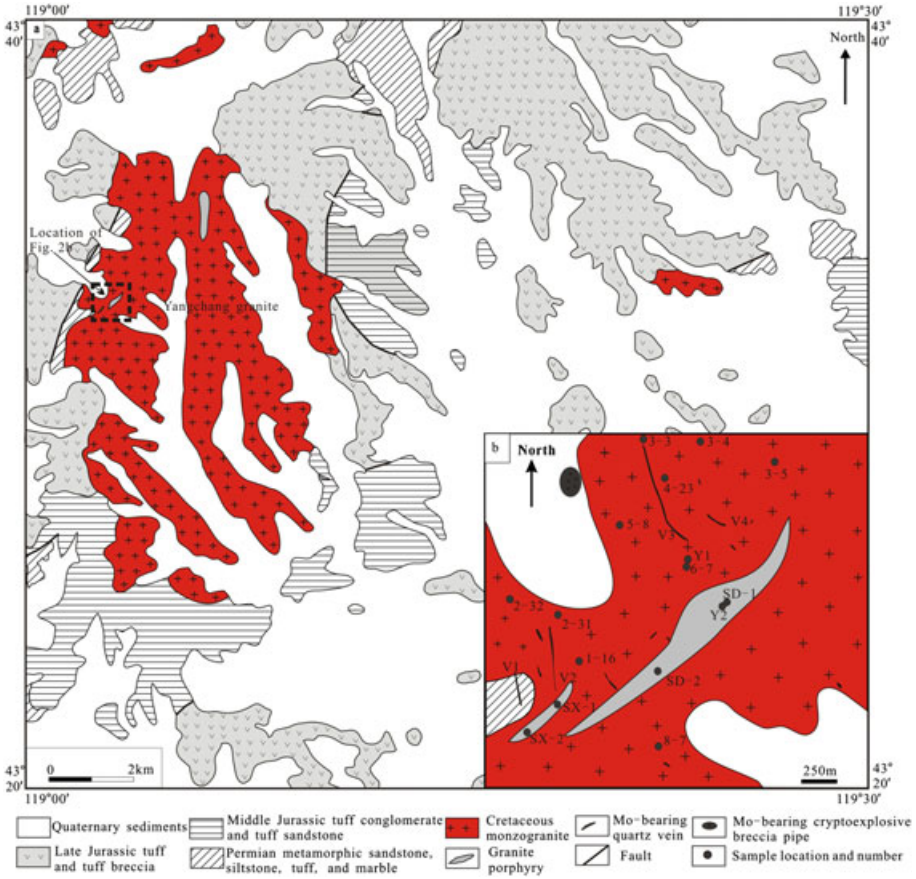


Figure 2. The geological map (a) and distribution map (b) of the Mo-bearing quartz veins of the Yangchang Mo deposit. Figure 2a modified from Bureau of Land and Mineral Resources of Chifeng (2008). This figure is available in colour online at wileyonlinelibrary.com/journal/gj

Cretaceous porphyritc granite (SHRIMP zircon U–Pb age: 139–142 Ma, Zeng *et al*., 2011a) contains 35–40% of phenocrysts and 55–60% of the matrix minerals. The phenocrysts include potash feldspar, plagioclase, quartz and biotite. The grain size of the phenocryst minerals changes from 2 to 3 mm. The matrix mineral assemblage is the same as that of the phenocrysts, but its grain size is 0.1 mm–0.5 mm. The accessory minerals are apatite, zircon, titanite, magnetite and allanite. The Cretaceous intrusions also intrude the Jurassic volcanics and Permian strata (Zeng *et al*., 2010a). The syenogranite porphyry is typically porphyritic, with crystals of orthoclase, which commonly represent ~5–15% of the rock. The matrix mineral assemblage includes quartz, orthoclase, plagioclase and biotite. Accessory minerals contain magnetite, zircon and apatite. The Yanshanian syenogranite porphyry often intrudes the Permian strata and the Paleozoic intrusions (Zeng *et al*., 2009).

The Yangchang Mo deposit is located in the Yangchang monzogranite batholith with an outcrop area of 50 $km^2$. The Yangchang monzogranite intruded into Permian metasediments, marble, Jurassic tuff and tuff breccia (Fig. 2a, b). This monzogranite body is intruded by granite porphyry dykes (Fig. 2a, b).

The Yangchang monzogranite is composed of K-feldspar (30–35%), plagioclase (30–35%), quartz (25%), biotite (5%) and hornblende (2–5%). K-feldspar is generally of perthitic texture. Plagioclase is generally euhedral and subhedral crystal, with polysynthetic twinning. Quartz is xenomorphic-granular, the brown biotite is schistose and the green hornblende is columnar. Accessory minerals include zircon, sphene and magnetite. The colourless zircons are euhedral and subhedral, short- to long-prismatic with aspect ratios of 1:1 to 2:1. Zircon size ranges from 100 to 250 μm.

The granite porphyry dykes are typically porphyritic textured, with crystals of quartz and orthoclase, which commonly represent 10% of the rock. The quartz is xenomorphic-granular, with a diameter of generally 0.2 mm. The orthoclase is of Carlsbad twin texture, with size ranging from 0.4 to 0.8 mm. The matrix is of microlitic texture, and the matrix mineral assemblage includes quartz, K-feldspar, plagioclase and biotite. Accessory minerals include magnetite, zircon and sphene. The colourless zircons are also euhedral

and subhedral, short- to long-prismatic with aspect ratios of 1:1 to 2:1. Zircon size ranges from 75 to 150 μm.

## 4. ANALYTICAL METHODS

Samples were crushed into granules less than 200 mesh and then analysed for major- and trace-elements and Sr–Nd–Pb isotopes. All of the analyses were carried out at the State Key Laboratory of Lithospheric Evolution in Beijing, Institute of Geology and Geophysics (IGG), Chinese Academy of Sciences (CAS). Major elements were determined by X-Ray Fluorescence (XRF), with analytical uncertainties ranging from 1% to 5%. Trace element and rare earth element concentrations were determined by inductively coupled plasma mass spectrometry (ICP-MS) with an ELEMENT system. According to Chinese national standards GSR-1 and GSR-2, the error was <5% for trace element with concentrations 10 ppm and <10% for trace element with concentrations <10 ppm (Gao *et al*., 2002).

Sr and Nd isotopes were analysed using a MAT-262 thermal ionization mass spectrometer (TIMS). About 100 mg of a whole-rock powder sample was weighed, and then appropriate amounts of $^{87}Rb$–$^{84}Rb$ and $^{149}Sm$–$^{150}Nd$ mixed diluent and purified HF–$HClO_4$ mixed acid were added so as to fully dissolve the sample at high temperature. Separation and purification were carried out in a quartz exchange column filled with 5 ml of AG 50 W-X12 exchange resin (200–400 mesh) for Rb and Sr and in a quartz exchange column with 1.7 ml of Teflon powder as an exchange medium for Sm and Nd. Isotope ratios of $^{146}Nd/^{144}Nd = 0.7219$ and $^{86}Sr/^{85}Sr = 0.1194$ were adopted for correction of obtained Nd and Sr isotope ratios, respectively. The results of standard samples BCR and NBS987 were $^{143}Nd/^{144}Nd = 0.512633 \pm 7$ ($n = 100$) and $^{87}Sr/^{86}Sr = 0.710244 \pm 4$ ($n = 100$), respectively. The blanks were about 100 pg for Rb and Sr and about 50 pg for Sm and Nd, respectively. The errors on $^{147}Sm/^{144}Nd$ and $^{87}Rb/^{86}Sr$ were less than 0.5%.

The Pb isotopes were analysed using a MAT-262 TIMS. HF acid was used to dissolve the sample, and the sample solution was dried by evaporation. A 6N HCI solution was employed to convert the fluorinated sample into chloride, which was dried by evaporation, and then 0.6N HBr was used for sample extraction. Flows of 0.6N HBr and 6N HCI were adopted to separate and purify the Pb sample in a Teflon exchange column filled with 80 μl of AGl × 8 (100–200 mesh) exchange resin. The result for the Pb standard sample NBS981 was $^{207}Pb/^{206}Pb = 0.9136$ ($n = 37$), and the whole-flow background for Pb was less than 50 pg (Chen *et al*., 2000, 2002).

Zircon grains were separated from two samples (Y1 and Y2) of the monzogranite and granite porphyry at the Yangchang deposit (Fig. 2b). Every sample is about 3.0 kg. Samples were crushed through 80–120 meshes, dust and magnetite were removed by washing and magnets, and then the zircons were separated using a conventional gravity method and handpicking at the Langfang Institute of Regional Investigation, Hebei Province. These zircon grains were mounted in epoxy, together with the 91 500 reference zircon (1065 Ma, uranium content: $81 \times 10^{-6}$; Wiedenbeck *et al*., 1995), which was used to calibrate U, Th and Pb concentrations. They were polished and photographed in transmitted light and cathodoluminescence (CL). The CL imaging was completed at the Electron Microprobe Laboratory in IGG, CAS.

U–Pb age determining was done using laser ablation ICP-MS. The ICP-MS is an Agilent 7500a (made by Agilent Co., USA), and the laser system is a GeoLas 2005 (made by Lambda Physik Co., Germany). The experimental conditions and the detailed procedures and principles are in Yuan *et al*. (2004) and Liu *et al*. (2008), respectively. The data were processed using the SQUID and ISOPLOT/Ex software of Ludwig (2003).

## 5. GEOCHEMISTRY

### 5.1. Major and trace elements

Major and trace element data for 14 rock samples including 10 monzogranite and four granite porphyry samples from the Yangchang ore area are listed in Table 1.

The monzogranites have high $SiO_2$ contents of 69–72 wt% and $Al_2O_3$ contents of 14–15 wt%, with $K_2O/Na_2O$ ratios of 0.69–0.92. They are metaluminous to slightly peraluminous with A/CNK of 0.98–1.03 and belong to the high-K calc-alkaline series (Fig. 3a, b). Granite porphyries have high $SiO_2$ contents of 77–79 wt% and low $Al_2O_3$ contents of 12–13 wt%, with high $K_2O/Na_2O$ ratios of 1.8–4.4 with respect to the monzogranitic rocks. Granite porphyries are peraluminous with A/CNK of 1.25–1.61 and also belong to the high-K calc-alkaline I-type granite series (Fig. 3a, b). The monzogranites have higher $Al_2O_3$, $TiO_2$, $Fe_2O_3$, FeO, MgO, CaO, $Na_2O$ and $P_2O_5$ and lower $K_2O$ contents than those of the granite porphyry (Table 1; Fig. 4). In the Harker diagrams, monzogranites and granite porphyries define a linear trend (Fig. 4).

The monzogranites have high Sr contents of 380–499 ppm and high Y concentrations of 14–18 ppm, with Sr/Y ratios of 22.7–35.5. The granite porphyries have low Sr contents of 30.5–71.1 ppm and low concentrations of 7.8–11.0 ppm, with low Sr/Y ratios of 4.1–7.4 with respect to the monzogranitic rocks (Table 1).

The monzogranites and granite porphyries are enriched in light rare earth elements (LREEs) and depleted in high rare earth elements (HREEs) (i.e. Yb = 0.8–2.1 ppm) and $(La/Yb)_{CN}$

Table 1. Whole rock major-, trace and REE element analyses of the Yangchang granitic rocks

| Sample no. | 1-16 | 2-31 | 2-32 | 3-3 | 3-4 | 3-5 | 4-23 | 5-8 | 6-7 | 8-7 | SD-1 | SD-2 | SX-1 | SX-2 |
|---|---|---|---|---|---|---|---|---|---|---|---|---|---|---|
| $SiO_2$ (Wt%) | 70.01 | 71.36 | 71.01 | 70.65 | 71.05 | 70.89 | 71.59 | 70.03 | 69.42 | 68.74 | 77.09 | 77.62 | 78.69 | 77.59 |
| $TiO_2$ | 0.36 | 0.31 | 0.32 | 0.38 | 0.34 | 0.34 | 0.31 | 0.34 | 0.40 | 0.38 | 0.08 | 0.08 | 0.07 | 0.08 |
| $Al_2O_3$ | 15.16 | 14.15 | 14.83 | 14.93 | 14.65 | 14.91 | 14.71 | 15.01 | 14.87 | 15.37 | 13.13 | 12.78 | 12.45 | 13.19 |
| $Fe_2O_3$ | 1.29 | 1.16 | 1.19 | 1.42 | 1.19 | 1.15 | 1.15 | 1.21 | 1.56 | 1.38 | 0.59 | 0.47 | 0.50 | 0.54 |
| FeO | 1.30 | 1.28 | 1.19 | 1.28 | 1.36 | 1.17 | 1.14 | 1.33 | 1.52 | 1.56 | 0.12 | 0.21 | 0.08 | 0.09 |
| MnO | 0.07 | 0.07 | 0.07 | 0.07 | 0.06 | 0.06 | 0.07 | 0.07 | 0.07 | 0.07 | 0.03 | 0.02 | 0.01 | 0.01 |
| MgO | 1.00 | 0.92 | 0.90 | 1.03 | 0.99 | 0.91 | 0.90 | 0.99 | 1.35 | 1.34 | 0.15 | 0.15 | 0.22 | 0.22 |
| CaO | 2.45 | 2.26 | 2.25 | 2.58 | 2.35 | 2.27 | 2.29 | 2.28 | 2.83 | 3.00 | 0.10 | 0.18 | 0.09 | 0.10 |
| $Na_2O$ | 4.32 | 4.13 | 4.16 | 4.27 | 4.00 | 4.05 | 4.05 | 4.09 | 3.94 | 4.04 | 2.85 | 2.73 | 1.18 | 1.50 |
| $K_2O$ | 3.26 | 3.19 | 3.59 | 2.96 | 3.22 | 3.71 | 3.19 | 3.66 | 3.30 | 3.13 | 4.98 | 4.96 | 5.21 | 5.47 |
| $P_2O_5$ | 0.12 | 0.12 | 0.11 | 0.13 | 0.12 | 0.11 | 0.11 | 0.13 | 0.13 | 0.13 | 0.01 | 0.01 | 0.01 | 0.01 |
| LOI | 0.52 | 0.54 | 0.38 | 0.34 | 0.44 | 0.42 | 0.42 | 0.62 | 0.40 | 0.80 | 0.90 | 0.84 | 1.36 | 1.38 |
| Total | 99.87 | 99.49 | 99.99 | 100.05 | 99.77 | 99.99 | 99.92 | 99.76 | 99.79 | 99.94 | 100.04 | 100.05 | 99.88 | 100.20 |
| $Na_2O + K_2O$ | 7.58 | 7.32 | 7.75 | 7.23 | 7.22 | 7.76 | 7.24 | 7.75 | 7.24 | 7.17 | 7.83 | 7.69 | 6.39 | 6.97 |
| $K_2O$ / $Na_2O$ | 0.75 | 0.77 | 0.86 | 0.69 | 0.81 | 0.92 | 0.79 | 0.89 | 0.84 | 0.77 | 1.75 | 1.81 | 4.42 | 3.65 |
| A/CNK | 1.00 | 0.99 | 1.00 | 1.00 | 1.02 | 1.01 | 1.03 | 1.01 | 0.98 | 0.99 | 1.28 | 1.25 | 1.61 | 1.54 |
| $Fe_2O_3$/FeO | 0.99 | 0.91 | 1.00 | 1.11 | 0.88 | 0.98 | 1.01 | 0.91 | 1.03 | 0.88 | 4.92 | 2.24 | 6.25 | 6.00 |
| La (ppm) | 28.75 | 24.87 | 27.02 | 34.40 | 29.36 | 29.86 | 23.71 | 29.64 | 29.82 | 34.92 | 22.53 | 22.31 | 8.36 | 13.57 |
| Ce | 57.62 | 49.99 | 53.88 | 69.62 | 56.36 | 59.55 | 48.78 | 55.98 | 53.53 | 56.90 | 35.81 | 35.18 | 16.92 | 25.74 |
| Pr | 6.81 | 6.01 | 6.36 | 7.99 | 6.49 | 6.55 | 6.01 | 6.51 | 6.02 | 5.95 | 3.94 | 4.05 | 1.43 | 2.49 |
| Nd | 23.76 | 20.80 | 22.34 | 27.74 | 23.13 | 22.91 | 21.65 | 23.03 | 20.79 | 19.96 | 12.24 | 12.84 | 4.35 | 7.49 |
| Sm | 3.79 | 3.29 | 3.56 | 4.40 | 3.53 | 3.91 | 3.50 | 3.71 | 3.51 | 3.27 | 1.86 | 1.97 | 0.65 | 1.19 |
| Eu | 0.80 | 0.72 | 0.76 | 0.83 | 0.77 | 0.82 | 0.76 | 0.82 | 0.84 | 0.84 | 0.26 | 0.26 | 0.11 | 0.19 |
| Gd | 3.24 | 2.82 | 3.06 | 3.73 | 3.25 | 3.27 | 2.90 | 3.09 | 3.20 | 2.95 | 1.74 | 1.74 | 0.61 | 1.00 |
| Tb | 0.46 | 0.41 | 0.45 | 0.53 | 0.44 | 0.44 | 0.43 | 0.43 | 0.44 | 0.39 | 0.24 | 0.27 | 0.10 | 0.16 |
| Dy | 2.73 | 2.36 | 2.59 | 3.01 | 2.59 | 2.66 | 2.51 | 2.65 | 2.45 | 2.31 | 1.38 | 1.55 | 0.65 | 1.02 |
| Ho | 0.56 | 0.50 | 0.56 | 0.65 | 0.56 | 0.55 | 0.53 | 0.54 | 0.52 | 0.49 | 0.30 | 0.34 | 0.16 | 0.24 |
| Er | 1.63 | 1.48 | 1.59 | 1.87 | 1.61 | 1.63 | 1.54 | 1.60 | 1.55 | 1.40 | 0.92 | 1.04 | 0.55 | 0.78 |
| Tm | 0.27 | 0.24 | 0.26 | 0.29 | 0.26 | 0.26 | 0.24 | 0.25 | 0.26 | 0.23 | 0.16 | 0.18 | 0.10 | 0.14 |
| Yb | 1.81 | 1.60 | 1.82 | 2.07 | 1.83 | 1.75 | 1.63 | 1.75 | 1.68 | 1.60 | 1.22 | 1.36 | 0.81 | 1.10 |
| Lu | 0.29 | 0.27 | 0.29 | 0.33 | 0.29 | 0.27 | 0.25 | 0.29 | 0.28 | 0.25 | 0.21 | 0.23 | 0.15 | 0.20 |
| ΣREE | 132.5 | 115.4 | 124.5 | 157.5 | 130.5 | 134.4 | 114.4 | 130.3 | 124.9 | 131.5 | 82.80 | 83.31 | 34.96 | 55.32 |
| LREE/HREE | 11.07 | 10.92 | 10.73 | 11.62 | 11.06 | 11.42 | 10.42 | 11.29 | 11.04 | 12.67 | 12.43 | 11.44 | 10.14 | 10.91 |
| δEu | 0.68 | 0.71 | 0.69 | 0.61 | 0.68 | 0.68 | 0.71 | 0.72 | 0.76 | 0.81 | 0.44 | 0.42 | 0.54 | 0.52 |
| (La/Yb)N | 11.39 | 11.13 | 10.68 | 11.91 | 11.52 | 12.22 | 10.43 | 12.17 | 12.71 | 15.69 | 13.29 | 11.80 | 7.44 | 8.84 |
| Y(ppm) | 15.61 | 14.30 | 15.42 | 17.86 | 15.17 | 15.6 | 14.47 | 15.11 | 14.53 | 14.04 | 9.67 | 10.94 | 4.90 | 7.78 |
| Zr | 164.6 | 143.3 | 171.9 | 158.7 | 157.8 | 137.7 | 137.5 | 162.0 | 155.8 | 139.9 | 73.03 | 74.42 | 68.47 | 71.52 |
| Hf | 4.92 | 4.29 | 5.06 | 4.79 | 4.71 | 4.13 | 4.06 | 4.96 | 4.81 | 4.19 | 3.42 | 3.38 | 3.07 | 3.16 |
| Cr | 2.77 | 2.66 | 2.61 | 4.4 | 3.68 | 3.94 | 7.62 | 3.77 | 17.22 | 15.69 | 0.46 | 0.48 | 0.46 | 2.29 |
| Co | 5.42 | 5.04 | 4.81 | 5.59 | 5.79 | 5.06 | 4.64 | 5.12 | 7.59 | 7.63 | 1.02 | 0.77 | 0.8 | 1.12 |
| Ni | 1.74 | 0.24 | 1.69 | 3.37 | 0.89 | 0.54 | 3.6 | 1.31 | 6.82 | 5.08 | 1.99 | 0.74 | 0.67 | 1.53 |
| Ga | 18.00 | 17.08 | 17.10 | 18.12 | 17.83 | 17.11 | 16.93 | 17.77 | 18.17 | 18.62 | 17.12 | 16.48 | 14.42 | 16.53 |
| Rb | 114.0 | 115.5 | 126.0 | 101.0 | 122.5 | 115.2 | 102.4 | 125.2 | 100.6 | 87.5 | 221.5 | 212.0 | 230.0 | 243.1 |
| Sr | 409.5 | 387.7 | 379.6 | 404.6 | 390.1 | 393.6 | 385.1 | 397.6 | 448.9 | 498.6 | 71.1 | 66.2 | 30.5 | 31.6 |
| Nb | 9.97 | 8.73 | 9.61 | 10.19 | 8.99 | 9.59 | 8.32 | 9.18 | 8.44 | 8.31 | 16.85 | 16.9 | 14.31 | 16.7 |
| Cs | 4.22 | 4.28 | 4.45 | 4.84 | 6.69 | 4.77 | 3.54 | 4.66 | 2.67 | 2.11 | 4.23 | 4.34 | 5.04 | 5.86 |
| Ba | 506.5 | 418.0 | 630.1 | 468.0 | 424.6 | 660.5 | 448.0 | 716.4 | 651.0 | 649.5 | 224.6 | 263.1 | 214.4 | 258.6 |
| Ta | 1.03 | 0.89 | 0.99 | 1.10 | 0.95 | 1.03 | 0.88 | 0.97 | 0.91 | 0.90 | 1.72 | 1.71 | 1.44 | 1.68 |
| Pb | 10.33 | 10.52 | 11.59 | 10.04 | 10.71 | 11.82 | 11.85 | 13.15 | 11.45 | 11.58 | 31.36 | 22.16 | 17.84 | 23.28 |
| Th | 17.9 | 19.75 | 22.25 | 27.87 | 21.51 | 20.06 | 19.37 | 20.6 | 15.26 | 17.26 | 25.47 | 25.73 | 21.53 | 23.86 |
| U | 2.74 | 3.06 | 2.87 | 3.8 | 2.73 | 2.73 | 3.95 | 4.87 | 4.32 | 3.69 | 5.37 | 4.99 | 4.52 | 4.27 |
| Sr/Y | 26.24 | 27.12 | 24.63 | 22.65 | 25.71 | 25.24 | 26.61 | 26.31 | 30.90 | 35.50 | 7.35 | 6.05 | 6.22 | 4.06 |

Note: Monzogranite:1-16, 2-31, 2-32, 3-3, 3-4, 3-5, 4-23, 5-8, 6-7, 8-7; granite porphyry: SD-1, SD-2; SX-1, SX-2. A/CNK = Al/(Ca + Na + K) molar; A/NK = Al/(Na + K) molar; LOI = Loss-on-ignition.

values of 7.4–15.7. In the rare earth element (REE) spider diagrams (Boynton, 1984), monzogranites and granite porphyries show concave-up REE patterns with differentiation of light–heavy rare earth elements with negative Eu anomalies (Fig. 5a, b). The monzogranites and granite porphyries have Eu/Eu* values of 0.61–0.81 and 0.42–0.54, respectively.

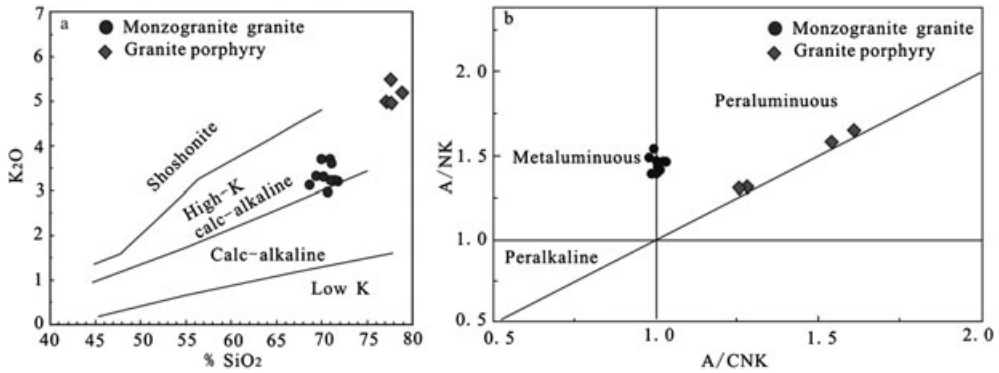


Figure 3. (a) Diagram of $SiO_2$ (%) versus $K_2O$ (%); (b) Diagram of A/CNK versus A/NK (Shand, 1927; Clarke, 1992).

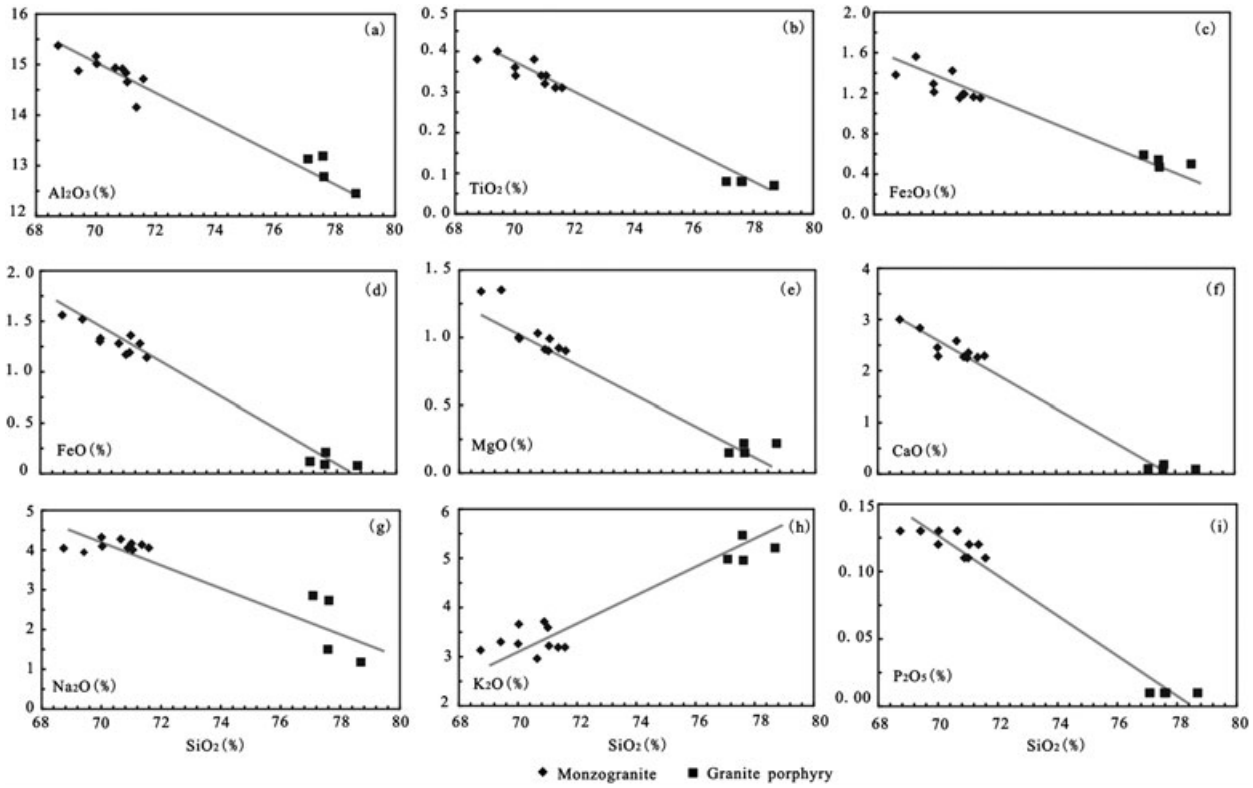


Figure 4. Plots of (a), $Al_2O_3$, (b), $TiO_2$, (c), $Fe_2O_3$, (d), FeO, (e), MgO, (f), CaO, (g), $Na_2O$, (h) , $K_2O$, and (i), $P_2O_5$ versus $SiO_2$ diagrams for monzogranites and granite porphyries from the Yangchang granitic intrusion.

In the primitive-mantle-normalized spidergrams (Sun and McDonough, 1989) monzogranites and granite porphyries are enriched in large-ion lithophile elements (LILEs), such as Rb, Th, U, K and Th, and depleted in high-field-strength elements (HFSEs), such as Nb, Ta, P and Ti (Fig. 6).

### 5.2. *Sr–Nd–Pb isotopes*

The Sr–Nd and Pb isotopic compositions of the Yangchang granitoids are listed in Tables 2 and 3 and are shown in Figures 7 and 8. The monzogranites have relatively low initial $^{87}Sr/^{86}Sr$ ratios (0.704573–0.705627) and relatively homogeneous $^{143}Nd/^{144}Nd$ ratios (0.512358–0.512385), with $\varepsilon_{Nd}(t)$ values of −2.0 to −1.5. The granite porphyry has low initial $^{87}Sr/^{86}Sr$ ratio (0.704281) and $^{143}Nd/^{144}Nd$ ratio (0.512285), with an $\varepsilon_{Nd}(t)$ value of −3.7. The monzogranites have $^{206}Pb/^{204}Pb$, $^{207}Pb/^{204}Pb$ and $^{208}Pb/^{204}Pb$ ratios of 18.73–18.98, 15.54–15.59 and 38.66–39.21, respectively. The granite porphyries have $^{206}Pb/^{204}Pb$, $^{207}Pb/^{204}Pb$ and $^{208}Pb/^{204}Pb$ ratios of 18.48–18.71, 15.53–15.60 and 38.44–38.54, respectively.

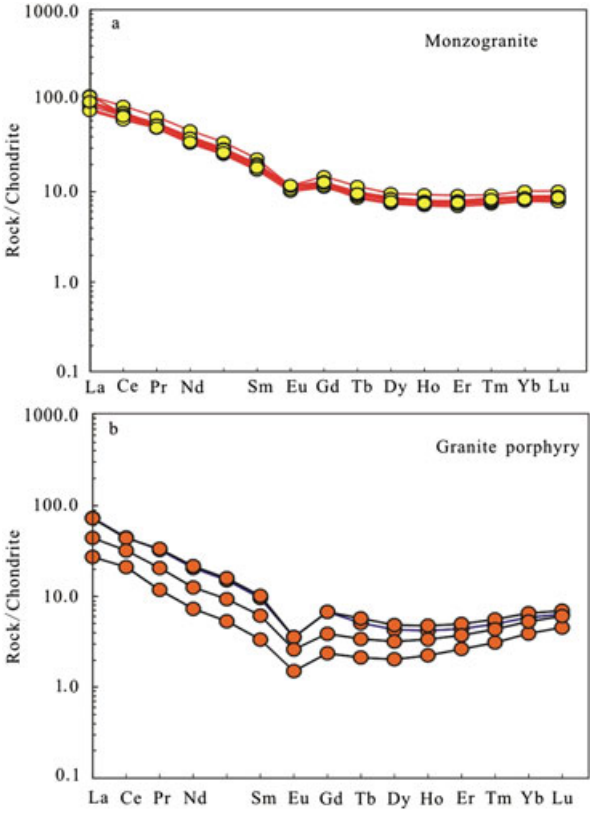


Figure 5. Chondrite-normalized REE patterns of the Yangchang granitic intrusion (normalization values after Boynton, 1984). This figure is available in colour online at wileyonlinelibrary.com/journal/gj

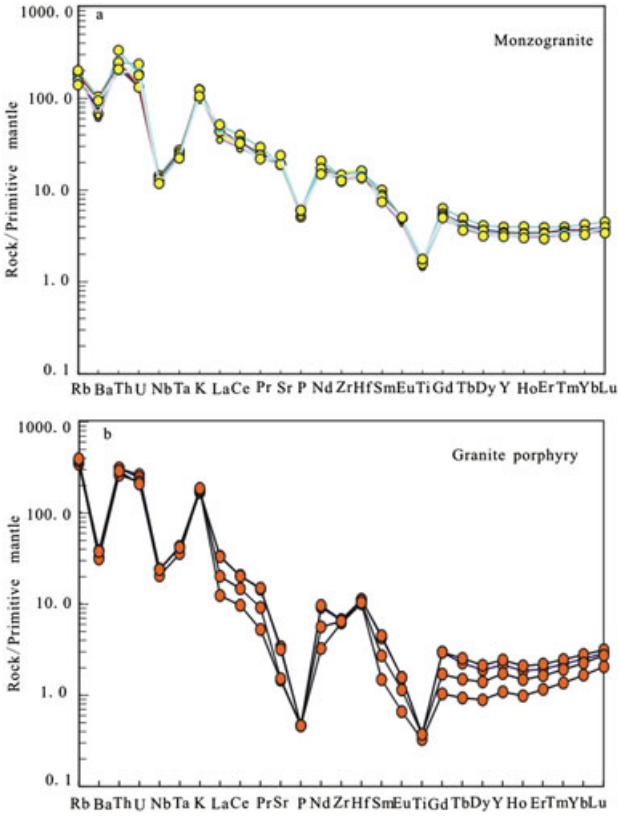


Figure 6. Primitive mantle-normalized trace elements spidergram of the Yangchang granitic intrusion (normalization values after Sun and McDonough, 1989). This figure is available in colour online at wileyonlinelibrary.com/journal/gj

The Yangchang granitoids have Sr–Nd isotopic compositions similar to those of the granitoids from the Phanerozoic and Neoproterozoic microcontinent massifs in the Central Asia Orogenic Belt (Wu *et al*., 1999; Hong *et al*., 2000, 2003) but distinct from the basement rocks of the North China Craton (Jahn *et al*., 1999) (Fig. 7).

## 6. GEOCHRONOLOGY

The cathodoluminescence (CL) images of zircons for Yangchang granitoids are shown in Figure 9. The U–Pb zircon data from the Yangchang monzogranite and granite porphyry are listed in Table 4 and shown in Figure 10.

Zircon grains from the monzogranite sample (Y1 ) have medium to high U contents (65–720 ppm) and low to high Th contents (11–810 ppm) (Table 4) with Th/U 0.34–1.22, possibly indicating a magmatic origin (Wu and Zheng, 2004). Only grain 1.22 has a very low Th/U ratio of 0.04.

The 22 zircon grains are concordant with a weighted mean $^{206}Pb/^{238}U$ age of $138 \pm 2$ Ma (MSWD = 0.69). The concordia age of 21 (excluding the 19) is $138 \pm 1$ Ma (MSWD = 0.0006). The mean age is consistent with the concordia age. This age is interpreted to be the crystallization age of the monzogranite.

Zircon grains from the granite porphyry (Y2) have U and Th concentrations of 206–917 ppm and 157–792 ppm, respectively, with Th/U ratios of 0.48–1.09 (Table 4), also indicating a magmatic origin. Sixteen analyses give ages between 129 and 139 Ma. They plot on a concordia curve with a weighted mean $^{206}Pb/^{238}U$ age of $132 \pm 2$ Ma (MSWD = 0.54), the concordia age is $132 \pm 1$ Ma (MSWD = 0.0038). The mean age is also consistent with the concordia age, indicating the crystallization age of the granite porphyry.

## 7. DISCUSSION

### 7.1. *Petrogenesis of Yangchang granitoids*

The Yangchang granitoids are characterized by relatively high silica and low FeO – MgO concentrations. They are calc-alkaline compositions (Fig. 3a). They are enriched in LILEs, such as Rb, K, U and Th, and depleted in HFSEs, such as Nb, Ta, Ti and P. They have relatively low initial $^{87}Sr/^{86}Sr$ ratios of 0.7043–0.7056 and weak negative $\varepsilon_{Nd}(t)$ (−1.5 to −3.7).

The monzogranites are metaluminous and have geochemical features of I-type granitoids, whereas the granite porphyries are peraluminous and have characteristics of the S-type granite. However, the granite porphyries mainly contain quartz and

Table 2. The Sr–Nd isotopic values of the Yangchang granitic rocks

| Sample no. | Sample description | $^{87}Rb/^{86}Sr$ | $^{87}Sr/^{86}Sr$ | $(^{87}Sr/^{86}Sr)i$ | $^{147}Sm/^{144}Nd$ | $^{143}Nd/^{144}Nd$ | $(^{143}Nd/^{144}Nd)i$ | $\varepsilon_{Nd}(t)$ | $f_{Sm/Nd}$ | $T_{DM}$(Ma) |
|---|---|---|---|---|---|---|---|---|---|---|
| 1-16 | Monzogranite | 0.7992 | 0.707109 | 0.705546 | 0.0982 | 0.512459 | 0.512371 | −1.8 | −0.50 | 914 |
| 2-31 | Monzogranite | 0.9214 | 0.707281 | 0.705479 | 0.1007 | 0.512476 | 0.512385 | −1.5 | −0.49 | 911 |
| 2-32 | Monzogranite | 0.9560 | 0.706443 | 0.704573 | 0.1007 | 0.512461 | 0.512371 | −1.8 | −0.49 | 931 |
| 3-3 | Monzogranite | 0.7372 | 0.706914 | 0.705472 | 0.1010 | 0.512453 | 0.512362 | −1.9 | −0.49 | 944 |
| 3-4 | Monzogranite | 0.9143 | 0.707331 | 0.705543 | 0.0964 | 0.512457 | 0.512370 | −1.8 | −0.51 | 903 |
| 3-5 | Monzogranite | 0.8772 | 0.707174 | 0.705459 | 0.0999 | 0.512457 | 0.512367 | −1.8 | −0.49 | 931 |
| 4-23 | Monzogranite | 0.7607 | 0.707000 | 0.705512 | 0.0998 | 0.512447 | 0.512358 | −2.0 | −0.49 | 942 |
| 5-8 | Monzogranite | 0.9489 | 0.707378 | 0.705522 | 0.0990 | 0.512454 | 0.512365 | −1.9 | −0.50 | 927 |
| 6-7 | Monzogranite | 0.6587 | 0.706916 | 0.705627 | 0.1021 | 0.512452 | 0.512360 | −2.0 | −0.48 | 955 |
| 8-7 | Monzogranite | 0.5047 | 0.706546 | 0.705559 | 0.1006 | 0.512460 | 0.512370 | −1.8 | −0.49 | 932 |
| SD-1 | Granite porphyry | 8.7742 | 0.720093 | 0.704281 | 0.0951 | 0.512364 | 0.512285 | −3.7 | −0.52 | 1012 |

Table 3. Pb isotopic values of the Yangchang granitic rocks

| Sample no. | Sample description | $^{206}Pb/^{204}Pb$ | 2σ | $^{207}Pb/^{204}Pb$ | 2σ | $^{208}Pb/^{206}Pb$ | 2σ |
|---|---|---|---|---|---|---|---|
| 1-16 | Monzogranite | 18.833 | 0.012 | 15.561 | 0.013 | 38.826 | 0.013 |
| 2-32 | Monzogranite | 18.805 | 0.018 | 15.540 | 0013 | 38.817 | 0.017 |
| 3-3 | Monzogranite | 18.983 | 0.007 | 15.566 | 0.007 | 39.212 | 0.007 |
| 3-4 | Monzogranite | 18.783 | 0.010 | 15.540 | 0.011 | 38.951 | 0.010 |
| 3-5 | Monzogranite | 18.727 | 0.008 | 15.555 | 0.009 | 38.844 | 0.008 |
| 4-23 | Monzogranite | 18.788 | 0.026 | 15.585 | 0.026 | 38.898 | 0.026 |
| 5-8 | Monzogranite | 18.824 | 0.014 | 15.550 | 0.014 | 38.821 | 0.014 |
| 6-7 | Monzogranite | 18.749 | 0.013 | 15.536 | 0.017 | 38.658 | 0.014 |
| 8-7 | Monzogranite | 18.777 | 0.026 | 15.572 | 0.025 | 38.822 | 0.025 |
| SD-1 | Granite porphyry | 18.709 | 0.020 | 15.598 | 0.020 | 38.537 | 0.020 |
| SD-2 | Granite porphyry | 18.593 | 0.021 | 15.548 | 0.022 | 38.493 | 0.024 |
| SX-1 | Granite porphyry | 18.558 | 0.012 | 15.531 | 0.011 | 38.438 | 0.011 |
| SX-2 | Granite porphyry | 18.479 | 0.019 | 15.531 | 0.018 | 38.456 | 0.019 |

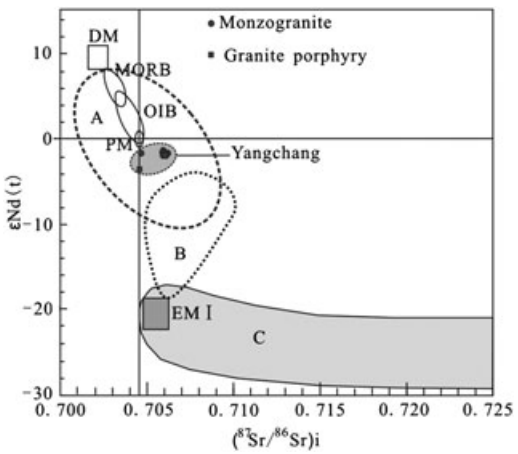


Figure 7. Diagram of $I_{Sr}$ versus $\varepsilon_{Nd}$ (t) of the Yangchang granitic intrusion DM, MORB, OIB, PM, EM I are defined by Hart (1984) and Zindler and Hart (1986). (A) granite in east segment of the Central Asia Orogenic Belt from Wu *et al*., 1999; (B) granite in northern margin of North China Craton is from the Zhou *et al*., 2001; (C) Precambrian basement is from Wu *et al*. 2005.

perthitic feldspar, with minor amounts of plagioclase, biotite (<5%) and other accessory minerals. They contain abundant miarolitic cavities, which suggest that they were emplaced at shallow levels with extensive fractional crystallization. Geochemically, the granite porphyries are silica-rich and peraluminous and have high alkali content. All these geochemical features of granite porphyries suggest that they are highly fractionated I-type granites (Wu *et al*., 2003). Furthermore, the monzogranites and granite porphyries have similar geochemical features and isotopic compositions, indicating their common sources. They have relatively low Sr and Ba contents and high Y and Yb concentrations with low Sr/Y ratios. They have relatively enriched LREEs and are depleted in HREEs (Eu/Eu* = 0.42–0.81), with $(La/Yb)_N$ values of 7.44–15.7. They have relatively young Nd model ages of 0.9–1.0 Ga and relatively low initial $^{87}Sr/^{86}Sr$ ratios with high Rb/Sr ratios ($^{87}Rb/^{86}Sr$ = 0.5047–8.774). All these geochemical features and isotopic compositions indicate that the Yangchang granitoids were derived from partial melting of juvenile crustal materials (with low initial $^{87}Sr/^{86}Sr$ ratios ($0.705 \pm 0.001$), high $\varepsilon_{Nd}(t)$ values (−3.7–4.0) and young $T_{DM}$ model ages (0.5–1.3 Ga), Wu *et al*., 2000) at a depth with plagioclase-rich residual assemblage (Martin and Nokes, 1989; Inger and Harris, 1993; Zhao *et al*., 2004). These geochemical features, similar to those of high-K calc-alkaline granitoids

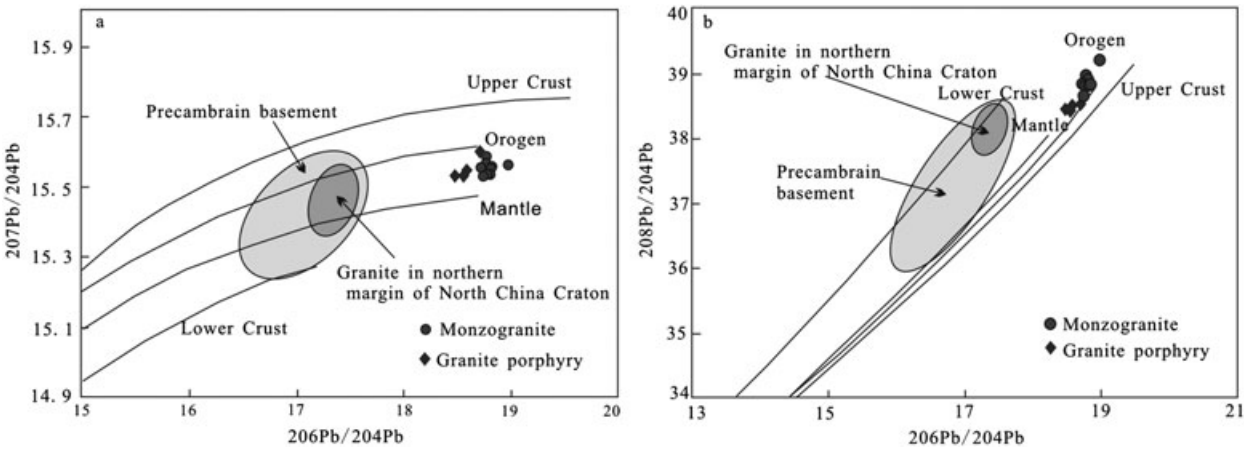


Figure 8. Diagram of Pb isotopic composition of the Yangchang granite on the growth curves from Zartman and Doe (1981). Data of Precambrian basement are from Chen *et al*. (1994), Li and Wang (1995); Data of granite in northern margin of North China Craton are from Zeng *et al*. (2011b).

in post-collision settings (Kuster and Harms, 1998; Liégeois *et al*., 1998), which were suggested to be derived from partial melting of junior crustal materials, may be the Neoproterozoic oceanic crust or accreted arc complex (Lin *et al*., 2004).

### *7.2. Genetic relationship between granitoids and Mo mineralization*

Porphyry Mo deposits, in comparison, are typically associated with felsic, high-silica ($72-77$ wt% $SiO_2$) and, in many cases, strongly differentiated granitic plutons (Mutschler *et al*., 1981; White *et al*., 1981; Kooiman *et al*., 1986). Subduction-related calc-alkaline rocks are related to the Endako-type (or arc-type) Mo deposit, and the alkaline rocks are related to the Climax-type (rift-type) Mo deposit (Sillitoe, 1980; Carten *et al*., 1993). Yangchang granitoids belong to high-K calc-alkaline rocks. The Yangchang Mo deposit is different from both the Endako-type Mo deposit and the Climax-type Mo deposit.

In the Yangchang ore area, field observations show that the Mo ore bodies occur spatially within the monzogranite and are cut by the granite porphyry (Fig. 2b). The Mo mineralization at Yangchang is localized in the monzogranite. Cryptoexplosive breccia-type and quartz-type mineralizations are recognized in the ore area. Quartz veins (0.1 to 2 m wide and 30 to 700 m long) include quartz and sulphide veins that have narrow sericitization zones (1–2 m). The quartz-vein mineralization is characterized by dissemination and veinlets of pyrite, molybdenite, chalcopyrite, galena and sphalerite. Breccia mineralization occurs within a steep cryptoexplosive breccia pipe. The compositions of breccia are mainly monzogranites. Ore minerals (molybdenite and pyrite) form part of the cement in these breccias. Sericitization and silicification are developed in the breccia pipe. The Yangchang Mo deposit can be classified as a granitic porphyry Mo deposit according to the classification scheme of Seedorff *et al*. (2005). Comparing with the well-known Climax Mo deposit in Colorado, USA (Wallace, 1995; Sinclair, 2007), we found that the Climax deposit and the Yangchang Mo deposits belong to the same deposit type, but there are interesting differences between the Climax and Yangchang deposits. For example, intrusive rocks related to Mo mineralization in the Climax deposit are rhyolite porphyry–granite porphyry, but Mo mineralization in the Yangchang deposit is related to the monzogranite.

The excellent correlation between the Re–Os date from molybdenite and ages of monzogranite from the area indicate a direct genetic relationship between the monzogranite intrusion and Mo mineralization. The Re–Os isochron age for molybdenites is $139 \pm 5$ Ma (Zeng *et al*., 2010b), the zircon U–Pb age of the monzogranite porphyry is $138 \pm 2$ Ma, and the zircon U–Pb age of the post ore granite porphyry is $132 \pm 2$ Ma. The $\delta^{34}S$ values of thirteen sulphides from the Yangchang deposit range from $-1.66‰$ to $1.29‰$ (with an average value of $0.52‰$) (unpublished data of the author); these $\delta^{34}S$ values are similar to $\delta^{34}S$ values of typical magmatic sulphide sulphur (Ohmoto, 1986), suggesting that ore-forming materials are magmatic in origin. The high silica contents and low MgO concentrations, with negative $\varepsilon_{Nd}(t)$ values and relatively young Nd model ages of about 1.0 Ga, suggest that the Yangchang granitoids were mainly derived from partial melting of junior crustal materials. Therefore, we infer that the Mo is derived from the junior crustal rocks. This result is consistent with the study of the source region of metals in porphyry deposits (Candela and Piccoli, 2005; Seedorff *et al*., 2005).

### *7.3. Tectonic implications*

Accretionary complexes are widely distributed along the eastern Asian continental margin. The existence of accretionary

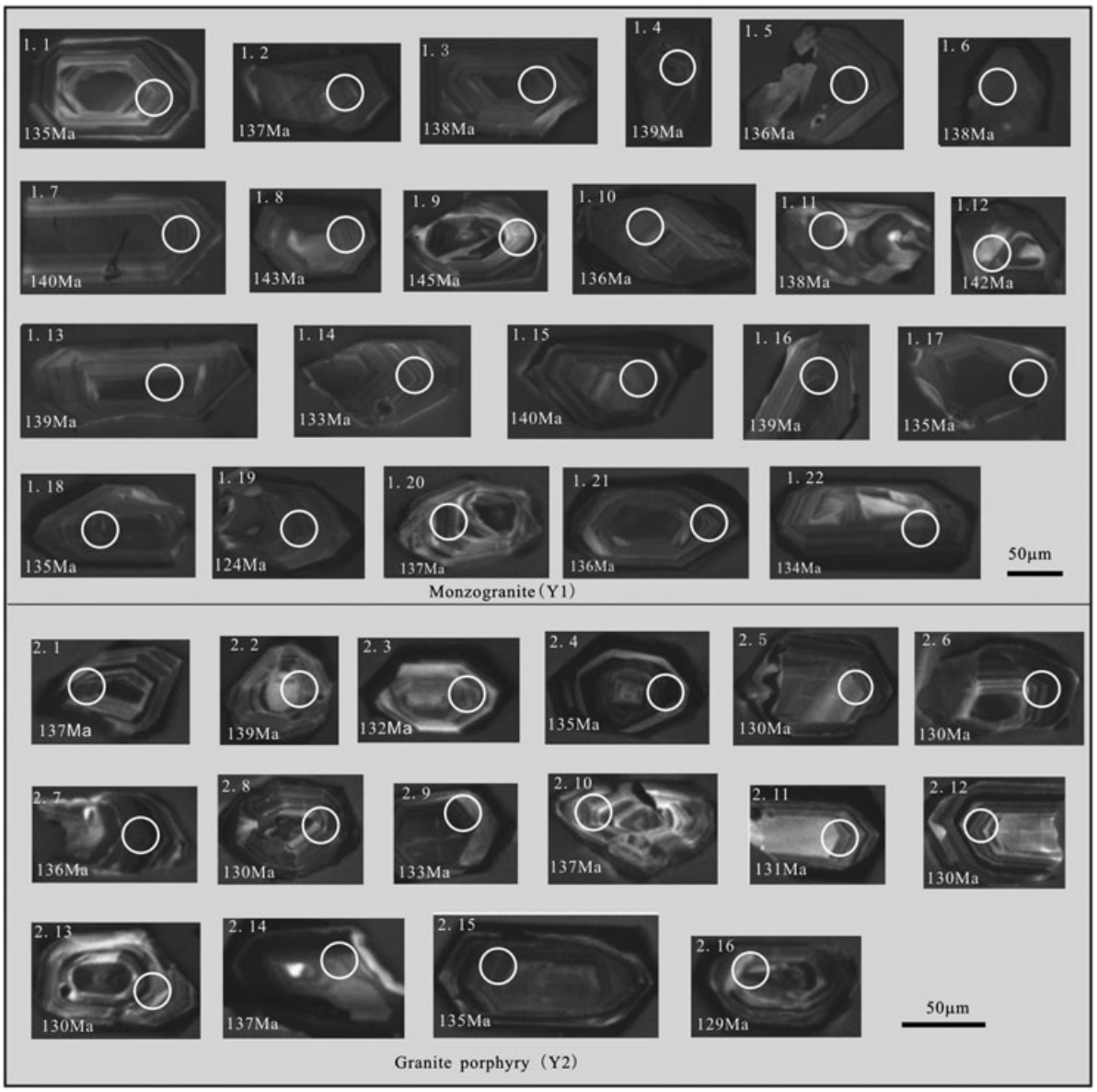


Figure 9. Cathodoluminescence (CL) images of zircons for Yangchang granitoids (Monzogranite (Y1), Granite porphyry (Y1)).

complexes indicates westward subduction of the Paleo-Pacific plate beneath the Euro-Asian plate in the Jurassic to Early Cretaceous (Natal'in and Borukayev, 1991; Natal'in, 1993; Sengör and Natal'in, 1996; Wakita and Metcalfe, 2005; Wu *et al*., 2007). The eastern Asian continental margin evolved in a subduction-related tectonic setting since at least the Early Jurassic (Wakita and Metcalfe, 2005; Wu *et al*., 2007).

The Yangchang granitoids mainly consist of monzogranite and granite porphyry. The geochemical features of granitoids indicate that the Cretaceous granitoids belong to the high-K calc-alkaline rock series. The calc-alkalic rocks are generally formed in subduction zones related to arc–continent or continental collision (Barbarin, 1999). Thus, the Yangchang granitoids were formed in the continental magma arc zone related to the subduction of the Paleo-Pacific plate under eastern China. The Yangchang monzogranites are calc-alkaline with relatively low $K_2O/Na_2O$ ratios, geochemical features similar to those of continental arc magmatism. The Yangchang granite porphyries have geochemical features similar to those of syn- or post-orogenic magmatism (Batchelor and Bowden, 1985). The trace element spider diagram shows enrichment in LILEs, impoverishment in HFSEs and depletions of Nb, Ta, P and Ti, all indicative of the trace element features of post-collision calc-alkalic and alkali-calcic type-I granite (Kuster and Harms, 1998). Shown in Figure 11 are data plots of Nb versus Y, Ta versus Yb, Rb versus Y + Nb

 

Table 4. Zircon U–Pb age data for the Yangchang granitic rocks

| Sample no. | $^{232}$Th(ppm) | $^{238}$U(ppm) | Th/U | $^{207}$Pb/$^{235}$U | 1σ | $^{206}$Pb/$^{238}$U | 1σ | $^{206}$Pb/$^{238}$U (Ma) | 1σ(Ma) |
|---|---|---|---|---|---|---|---|---|---|
| Monzogranite | (Y1) | | | | | | | | |
| 1.1 | 404 | 595 | 0.68 | 0.14209 | 0.01059 | 0.02112 | 0.00061 | 135 | 4 |
| 1.2 | 180 | 305 | 0.59 | 0.14376 | 0.00650 | 0.02146 | 0.00044 | 137 | 3 |
| 1.3 | 482 | 499 | 0.97 | 0.14462 | 0.00963 | 0.02159 | 0.00061 | 138 | 4 |
| 1.4 | 325 | 535 | 0.61 | 0.14842 | 0.00833 | 0.02184 | 0.00057 | 139 | 4 |
| 1.5 | 384 | 573 | 0.67 | 0.14295 | 0.00734 | 0.02130 | 0.00050 | 136 | 3 |
| 1.6 | 289 | 442 | 0.66 | 0.14575 | 0.00729 | 0.02165 | 0.00049 | 138 | 3 |
| 1.7 | 22 | 66 | 0.34 | 0.14743 | 0.00739 | 0.02188 | 0.00050 | 140 | 3 |
| 1.8 | 256 | 391 | 0.66 | 0.15103 | 0.00885 | 0.02242 | 0.00061 | 143 | 4 |
| 1.9 | 434 | 685 | 0.63 | 0.15416 | 0.01012 | 0.02278 | 0.00063 | 145 | 4 |
| 1.10 | 423 | 563 | 0.75 | 0.14342 | 0.00662 | 0.02131 | 0.00047 | 136 | 3 |
| 1.11 | 86 | 139 | 0.62 | 0.14438 | 0.00864 | 0.02159 | 0.00058 | 138 | 4 |
| 1.12 | 810 | 663 | 1.22 | 0.14975 | 0.01768 | 0.02225 | 0.00095 | 142 | 6 |
| 1.13 | 458 | 649 | 0.71 | 0.14612 | 0.00787 | 0.02176 | 0.00053 | 139 | 3 |
| 1.14 | 22 | 65 | 0.34 | 0.14011 | 0.01158 | 0.02087 | 0.00079 | 133 | 5 |
| 1.15 | 402 | 528 | 0.76 | 0.14762 | 0.01013 | 0.02199 | 0.00062 | 140 | 4 |
| 1.16 | 284 | 472 | 0.60 | 0.14724 | 0.01270 | 0.02181 | 0.00084 | 139 | 5 |
| 1.17 | 317 | 436 | 0.73 | 0.14333 | 0.01624 | 0.02119 | 0.00103 | 135 | 7 |
| 1.18 | 262 | 383 | 0.68 | 0.14206 | 0.00908 | 0.02116 | 0.00061 | 135 | 4 |
| 1.19 | 186 | 259 | 0.72 | 0.12925 | 0.01647 | 0.01944 | 0.00110 | 124 | 7 |
| 1.20 | 718 | 720 | 1.00 | 0.14476 | 0.01307 | 0.02153 | 0.00076 | 137 | 5 |
| 1.21 | 379 | 466 | 0.81 | 0.14246 | 0.01186 | 0.02134 | 0.00079 | 136 | 5 |
| 1.22 | 11 | 254 | 0.04 | 0.14215 | 0.00952 | 0.02107 | 0.00057 | 134 | 4 |
| Granite porphyry | (Y2) | | | | | | | | |
| 2.1 | 543 | 658 | 0.83 | 0.14164 | 0.01585 | 0.02143 | 0.00106 | 137 | 7 |
| 2.2 | 290 | 414 | 0.70 | 0.14858 | 0.03012 | 0.02185 | 0.00197 | 139 | 12 |
| 2.3 | 347 | 364 | 0.95 | 0.13917 | 0.01363 | 0.02068 | 0.00090 | 132 | 6 |
| 2.4 | 187 | 394 | 0.48 | 0.14169 | 0.00935 | 0.02110 | 0.00061 | 135 | 4 |
| 2.5 | 237 | 426 | 0.56 | 0.13544 | 0.01067 | 0.02030 | 0.00071 | 130 | 4 |
| 2.6 | 619 | 654 | 0.95 | 0.13607 | 0.00878 | 0.02030 | 0.00061 | 130 | 4 |
| 2.7 | 792 | 917 | 0.86 | 0.14139 | 0.01042 | 0.02126 | 0.00072 | 136 | 5 |
| 2.8 | 399 | 483 | 0.83 | 0.13731 | 0.01305 | 0.02035 | 0.00087 | 130 | 5 |
| 2.9 | 432 | 520 | 0.83 | 0.13988 | 0.00796 | 0.02087 | 0.00052 | 133 | 3 |
| 2.10 | 244 | 345 | 0.71 | 0.14332 | 0.01595 | 0.02147 | 0.00099 | 137 | 6 |
| 2.11 | 376 | 465 | 0.81 | 0.13750 | 0.01323 | 0.02058 | 0.00088 | 131 | 6 |
| 2.12 | 651 | 596 | 1.09 | 0.13577 | 0.00676 | 0.02029 | 0.00047 | 130 | 3 |
| 2.13 | 526 | 507 | 1.04 | 0.13727 | 0.00777 | 0.02041 | 0.00053 | 130 | 3 |
| 2.14 | 157 | 206 | 0.76 | 0.14436 | 0.01279 | 0.02149 | 0.00075 | 137 | 5 |
| 2.15 | 390 | 682 | 0.57 | 0.14212 | 0.00715 | 0.02110 | 0.00052 | 135 | 3 |
| 2.16 | 777 | 882 | 0.88 | 0.13619 | 0.00658 | 0.02024 | 0.00048 | 129 | 3 |

and Rb versus Yb + Nb for the volcanic arc granite and syn-collision granite area. The data suggest that all of the granitoids of the Yangchang batholith were formed within a compressional tectonic setting. The formation of the granitic rocks may be likely related to subduction of the Paleo-Pacific Ocean.

## 8. CONCLUSIONS

The Yangchang monzogranite and granite porphyry belong to a calc-alkaline rock series. The monzogranite and granite porphyry yield laser ablation ICP-MS U–Pb zircon ages of $138 \pm 2$ and $132 \pm 2$ Ma, respectively. The molybdenite ages of $139 \pm 5$ Ma from the Yangchang area indicate a close genetic relationship between monzogranite and the Mo metallogenesis.

The Cretaceous Mo-bearing granite at the east Central Asia Orogenic Belt was formed by partial melting of the Neoproterozoic junior crustal materials during the period of subduction of the Paleo-Pacific plate under east China.

## ACKNOWLEDGEMENTS

We sincerely thank the following organizations and people for their support and help: Guoying Mining Co. Ltd, Chifeng, which greatly supported our field work. We also

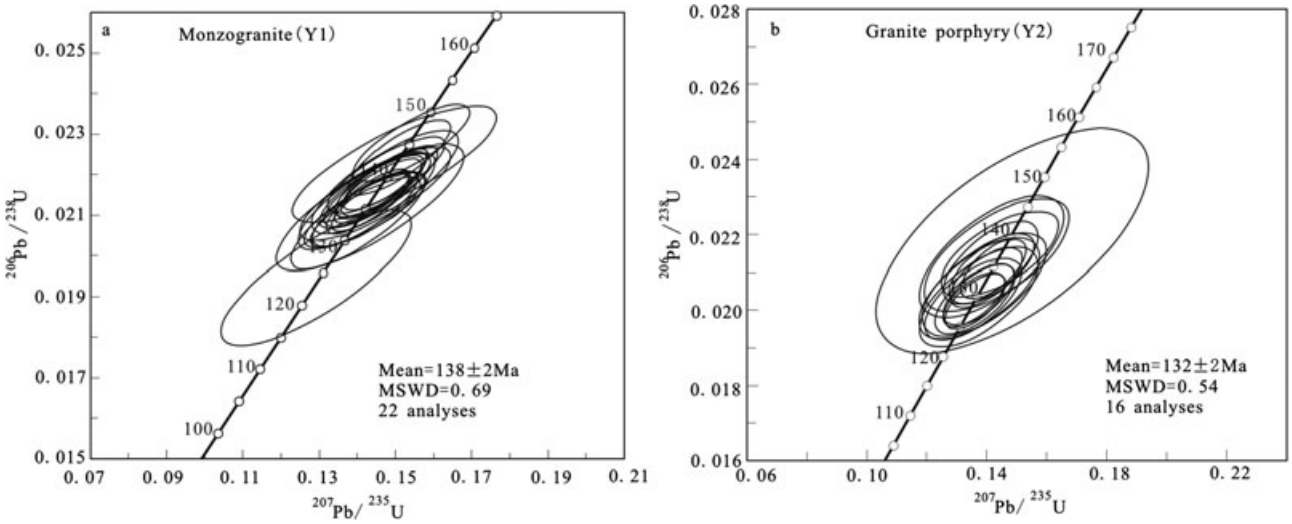


Figure 10. U–Pb zircon Concordia plots.

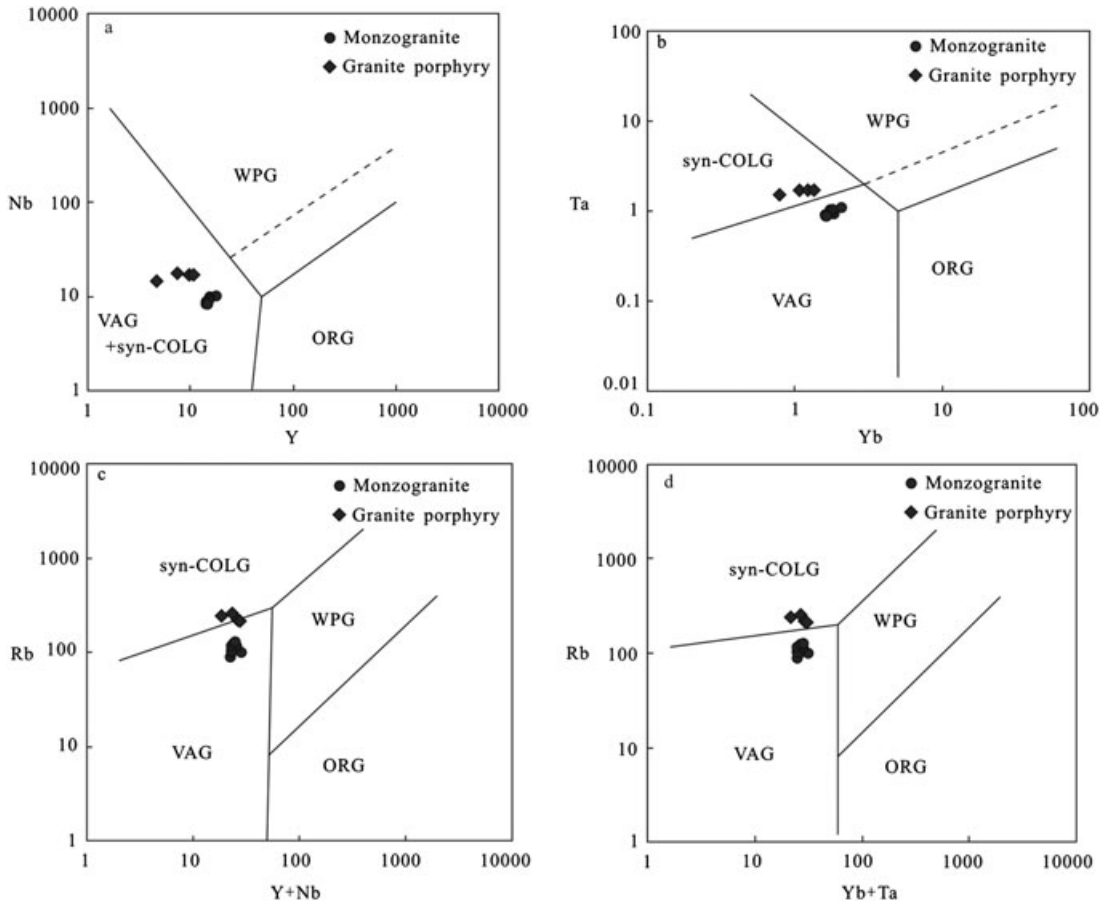


Figure 11. Diagrams of (a) Nb versus Y, (b) Ta versus Yb, (c) Rb versus Y + Nb and (d) Rb versus Yb + Nb (Pearce *et al*., 1984).

thank Dr Yang Yueheng for helping the LA-ICPMS U–Pb zircon dating test, senior engineer Li He for helping major element analysis of rocks, researcher Jin Xindi for helping the trace and rare earth element analysis of rocks, and Dr Chu Zhuoyin and Li Chaofeng for helping Sr–Nd–Pb isotope analysis. We sincerely thank Dr Ersin Koralay

and Dr Sibel Tatar Erkül for their detailed comments and constructive revision ideas. This work was financially supported by the Major State Basic Research Program of China (no. 2013 CB429800) and the National Natural Science Foundation of China (no. 40972065).

## REFERENCES

**Barbarin, B. 1999**. A review of the relationships between granitoid types, their origins and their geodynamic environments. *Lithos* **46**, 605–626.

**Batchelor, R.A., Bowden, P. 1985**. Petrogenetic interpretation of granitoid rock series using multicationic parameters. *Chemical Geology* **48**, 43–55.

**Boynton, W.V. 1984**. Cosmochemistry of rare earth elements: meteorite studies. In: *Rare Earth Element Geochemistry*, Henderson, P. (ed.). Elsevier: Amsterdam; 63–114.

**Bureau of Geology and Mineral Resources of Neimongol Autonomous Region (BGMR). 1991**. *Regional geology of Neimonggol Autonomous Region*. Geological Publishing House: Beijing; 1–532 (in Chinese).

**Bureau of Land and Mineral Resources of Chifeng. 2008**. Explanation on Geology and Mineral Resources of Zhaohuduge area in Chifeng, Inner Mongolia (scale: 1:50000); 1–32.

**Candela, P.A., Piccoli, P. 2005**. Magmatic processes in the development of porphyry-type ore systems. *Economic Geology* 100th Anniversary, 25–37.

**Carten, R.B., White, W.H., Stein, H.J. 1993**. High-grade granite-related molybdenum systems: classification and origin. In: *Geological Association of Canada Special Paper*, Kirkham, R.V., Sinclair, W.D., Thorpe, R.I., Duke, J.M. (eds). Mineral Deposit Modeling **40**, 521–544.

**Chen, Z.S., Zhang, L.G., Liu, J.X., Wang, B.C., Xu, J.F., Zheng, W.S. 1994**. A study on Lead isotope geochemical backgrounds of geological bodies in Jiaodong region. *Contributions to Geology and Mineral Resources Research* **10**(4), 65–78 (in Chinese with English abstract).

**Chen, F.K., Hegner, E., Todt, W. 2000**. Zircon ages, Nd isotopic and chemical compositions of orthogneisses from the Black Forest, Germany-evidence for a Cambrian magmatic arc. *International Journal of Earth Science* **88**, 791–802.

**Chen, F.K., Siebel, W., Satir, M., Terzioglu, N., Saka, K. 2002**. Geochronology of the Karadere basement (NW Turkey) and implications for the geological evolution of the Istanbul zone. *International Journal of Earth Science* **91**, 469–481.

**Clarke, D.B. 1992**. *Granitoid Rocks*. Chapman and Hall: London; 1–283

**Gao, S., Liu, X.M., Yuan, H.L., Hattendorf, B., Gunther, D., Chen, L., Hu, S.H. 2002**. Determination of forty two major and trace elements in USGS and NIST SRM glasses by laser ablation-inductively coupled plasma-mass spectrometry. *Geostandards Newsletter* **26**, 191–196.

**Hart, S.R. 1984**. A large-scale isotope anomaly in the Southern Hemisphere mantle. *Nature* **309**, 753–757.

**Hong, D.W., Wang, S.G., Xie, X.L., Zhang, J.S. 2000**. Genesis of positive $\varepsilon_{Nd}(t)$ granitoids in Da Hinggan Mountains–Mongolia orogenic belt and growth of continental crust. *Earth Science Frontiers* **7**(2), 441–456 (in Chinese with English abstract).

**Hong, D.W., Wang, S.G., Xie, X.L., Zhang, J.S., Wang, T. 2003**. Corelation between continental growth and the supercontinental cycle: evidence from the granites with positive $\varepsilon_{Nd}$ in the Central Asian orogenic belt. *Acta Geologica Sinica* **77**(2), 203–209 (in Chinese with English abstract).

**Inger, S., Harris N. 1993**. Geochemical constrains on leucogranite magmatism in the Langtang Valley, Nepal, Himalaya. *Journal of Petrology* **34**, 345–368.

**Jahn, B.M., Wu, F.Y., Lo, C.H., Tsai, C. 1999**. Crust–mantle interaction induced by deep subduction of the continental crust: geochemical and Sr–Nd istopic evidence from post-collisional mafic–ultramafic intrusions of the northern Dabie complex, central China. *Chemical Geology* **157**, 119–146.

**Kooiman, G.J.A., McLeod, M.J., Sinclair, W.D. 1986**. Porphyry tungsten–molybdenum orebodies, polymetallic veins and replacement bodies, and tin-bearing greisen zones in the Fire Tower Zone, Mount Pleasant, New Brunswick. *Economic Geology* **81**, 1356–1373.

**Kuster, D., Harms, U. 1998**. Post-collisional potassic granitoids from the southern and northwestern parts of the late Neo-proterozoic East African Orogen: a review. *Lithos* **45**, 177–195.

**Li, S.C., Wang, S.L. 1995**. Geochemical characteristics of gold deposits of north margin of the North China Continental Table, China. *Contributions to Geology and Mineral Resources Research* **10**(4), 8–19 (in Chinese with English abstract).

**Liégeois, J.P., Navez, J., Hertogen, J., Black, R. 1998**. Contrasting origin of post-collisional high-K calc-alkaline and shoshonitic versus alkaline and peralkaline granitoids. The use of sliding normalization. *Lithos* **45**, 1–28.

**Lin, Q., Ge, W.C., Wu, F.Y., Sun, D.Y., Cao, L. 2004**. Geochemistry of Mesozoic granites in Da Hinggan Ling rangs. *Acta Petrologica Sinica* **20**(3), 403–412 (in Chinese with English abstract).

**Liu, Y.S., Hu, Z.G., Gao, S., Gunther, D., Xu, J., Gao, C.C., Chen, H.H. 2008**. In situ analysis of major and elements of anhydrous minerals by LA-ICP-MS without applying an internal standard. *Chemical Geology* **257**(1–2), 34–43.

**Liu, J.M., Zhao, Y., Sun, Y.L., Li, D.P., Liu, J., Chen, B.L., Zhang, S.H., Sun, W.D. 2010**. Recognition of the latest Permian to Early Triassic Cu–Mo mineralization on the northern margin of the North China block and its geological significance. *Gondwana Research* **17**, 125–134.

**Ludwig, K.R. 2003**. Users manual for Isoplot 3.00: a geochronological toolkit for Microsoft Excel. *Berkley Geochronology Center Special Publication* **4**, 1–70.

**Martin, D., Nokes, R. 1989**. A fluid-dynamical study of crystal setting in convecting magma chambers. *Journal of Petrology* **30**, 1471–1500.

**Mutschler, F.E., Wright, E.G. Ludington, S., Abbott, J.T. 1981**. Granite molybdenite systems. *Economic Geology* **76**, 874–897.

**Natal'in, B.A. 1993**. History and models of Mesozoic accretion in southeastern Russia. *Island Arc* **2**, 12–34.

**Natal'in, B.A., Borukayev, C.B. 1991**. Mesozoic sutures in the southern far east of USSR. *Geotectonics* **25**, 64–74.

**Nie, F.J., Zhang, W.Y., Du, A.D., Jiang, S.H., Liu, Y. 2007**. Re–Os isotopic dating on molybdenite separates from the Xiaodonggou porphyry Mo deposit, Hexigten Qi, Mongolia. *Acta Geologica Sinica* **81**(7), 898–905 (in Chinese with English abstract).

**Ohmoto, H. 1986**. Stable isotope geochemistry of ore deposits. In: *Stable Isotopes in High Temperature Geological Processes*, Valley, J.W., Taylor, H.P., O'Neil, J.R. (eds). Mineral Soc. Am. Rev Mineral **16**, 491–557.

**Pearce, J.A., Harris, N.B.W., Tindle, A.G. 1984**. Trace element discrimination diagrams for the tectonic interpretation of granitic rocks. *Journal of Petrology* **25**, 956–983.

**Qin, F., Liu, J.M., Zeng, Q.D., Luo, Z.H. 2009**. Petrogenetic and metallogenic mechanism of the Xiaodonggou porphyry Molybdenum deposit in Hexigten Banner, Inner Mongolia. *Acta Petrologica Sinica* **25**(12), 3357–3368 (in Chinese with English abstract).

**Seedorff, E., Dilles, J.H., Proffett, Jr., J.M., Einaudi, M.T. 2005**. Porphyry deposits: characteristics and origin of hypogene features. *Economic Geology* **100th Anniversary**, 251–298.

**Sengör, A.M.C., Natal'in, B.A. 1996**. Paleotectonics of Asia: fragments of a synthesis. In: *The Tectonic Evolution of Asia*, Yin, A., Harrison, M. (eds). Cambridge University Press: Cambridge; 486–640.

**Shand, S.J. 1927**. *Eruptive Rocks*. Murby: London; 1-360.

**Sillitoe, R.H. 1980**. Types of porphyry molybdenum deposits. *Mining Magazine* **142**, 550–551, 553.

**Sinclair, W.D. 2007**. Porphyry deposits. In: *Mineral Deposits of Canada: a Synthesis of Major Deposit-Types, District Metallogeny, the Evolution of Geological Provinces, and Exploration Methods*, Goodfellow, W.D. (ed.). Geological Association of Canada. Mineral Deposits Division, Special Publication: St John's, Newfoundland; **5**, 223–24.

**Sun, S.S., McDonough, W.F. 1989**. Chemical and isotopic systematics of oceanic basalts; implications for mantle composition and processes. In: *Magmatism in the Ocean Basins*, Saunders, A.D., Norry, M.J. (eds). Geological Society of London: London; Special Publication **42**, 313–345.

**Wakita, K., Metcalfe, I. 2005**. Ocean plate stratigraphy in East and Southeast Asia. *Journal of Asian Earth Sciences* **24**, 679–702.

 

**Wallace S.R. 1995**. The Climax-type molybdenite deposits: what they are, where they are, and why they are. *Economic Geology* **90**, 1359–1380.

**White, W.H., Bookstrom, A.A., Kamilli, R.J., Ganster, M.W., Smith, R.P., Ranta, D.E., Steininger, R.C. 1981**. Character and origin of Climax-type molybdenum deposits. In: *Economic Geology Seventy-Fifth Anniversary Volume, 1905–1980*, Skinner, B.J. (ed.). Economic Geology Publishing Co: El Paso, Texas; 270–316.

**Wiedenbeck, M., Alle, P., Corfu, F., Griffin, W.L., Meier, M., Oberli, F., Vonquadt, A., Roddick, J.C., Peigel, W. 1995**. Three natural zircon standards for U–Th–Pb, Lu–Hf, trace-element and REE analyses. *Geostandards Newsletter* **19**, 1–23.

**Wu, Y., Zheng, Y., 2004**. Genesis of zircon and its constraints on interpretation of U–Pb age. *Chinese Science Bulletin* **49**(15), 1554–1569.

**Wu, F.Y., Sun, D.Y., Lin, Q. 1999**. Petrogenesis of the Phanerozoic granites and crustal growth in Northeast China. *Acta Petrologica Sinica* **15**(2), 181–189 (in Chinese with English abstract).

**Wu, F.Y., Jahn, B.M., Wilde, S., Sun, D.Y. 2000**. Phanerozoic crustal growth: U–Pb and Sr–Nd isotopic evidence from the granites in northeastern China. *Tectonophysics* **328**, 89–113.

**Wu, F.Y., Jahn, B.M., Wilde, S.A., Lo, C.H., Yui, T.F., Lin, Q., Ge, W. C., Sun, D.Y., 2003**. Highly fractionated I-type granites in NE China (I): Geochronology and petrogenesis. *Lithos* **66**, 241–273.

**Wu, F.Y., Yang, J.H., Wilde, S.A., Zhang, X.O. 2005**. Geochronology, petrogenesis and tectonic implications of Jurassic granites in the Liaodong Peninsula, NE China. *Chemical Geology* **221**, 127–156.

**Wu, F.Y., Zhao, G.C., Sun, D.Y., Wilde, S.A., Yang, J.H. 2007**. The Hulan Group: its role in the evolution of the Central Asian Orogenic Belt of NE China. *Journal of Asian Earth Sciences* **30**, 542–556.

**Wu, H.Y., Zhang, L.C., Chen, Z.G., Wan, B. 2008**. Geochemistry, tectonic setting and mineralization potentiality of the ore-bearing monzogranite in the Kulitu molybdenum (copper) deposit of Xar moron metallogetic belt. Inner Mongolia. *Acta Petrologica Sinica* **24**, 867–878 (in Chinese with English abstract).

**Wu, F.Y., Sun, D.Y., Ge, W.C., Zhang, Y.B., Grant, M.L., Wilde, S.A., Jahn, B.M. 2011a**. Geochronology of the Phanerozoic granitoids in northeastern China. *Journal of Asian Earth Sciences* **41**, 1–30.

**Wu, H.Y., Zhang, L.C., Wan, B., Chen, Z.G., Xiang, P., Pirajno, F., Du, A. D., Qu W.J. 2011b**. Re–Os and $^{40}Ar/^{39}Ar$ ages of the Jiguanshan porphyry Mo deposit, Xilamulun metallogenic belt, NE China, and constraints on mineralization events. *Mineralium Deposita* **46**, 171–185.

**Yuan, H.L., Gao, S., Liu, X.M., Li, H.M., Gunther, D., Wu, F.Y. 2004**. Accurate U–Pb age and trace element determinations of zircon by laser ablation-inductively coupled plasma mass spectrometry. *Geoanalytical and Geostandard Newsletters* **28**(3), 353–370.

**Zartman, R.E., Doe, B.R. 1981**. Plumbotectonics: the model. *Tectonophysics* **75**, 135–162.

**Zeng, Q.D., Liu, J.M., Zhang, Z.L., Qin, F., Cheng, W.J., Yu, C.M., Ye, J. 2009**. Ore forming time of the Jiguanshan Porphyry molybdenum deposit, north margin of North China Craton and the Indosinian mineralization. *Acta Petrologica Sinica* **25**(2), 393–398 (in Chinese with English abstract).

**Zeng, Q.D., Liu, J.M., Qin, F., Zhang, Z.L. 2010a**. Geochronology of the Xiaodonggou porphyry Mo deposit in northern margin of North China Craton. *Resource Geology* **60**(2), 192–202.

**Zeng, Q.D., Liu, J.M., Zhang, Z.L. 2010b**. Re–Os geochronology of porphyry molybdenum deposit in south segment of Da Hinggan Mountains, northeastern China. *Journal of Earth Sciences* **21**, 390–401

**Zeng, Q.D., Liu, J.M., Zhang, Z.L., Chen, W.J., Zhang, W.Q. 2011a**. Geology and geochronology of the Xilamulun molybdenum metallogenic belt in eastern Inner Mongolia, China. *International Journal of Earth Sciences* **100**, 1791–1809.

**Zeng, Q.D., Liu, J.M., Zhang, Z.L., Zhang, W.Q., Chu, S.X., Zhang, S., Wang Z.C., Duan, X.X. 2011b**. Geology, fluid inclusion, and sulfur isotope studies of the Chehugou porphyry molybdenum–copper deposit, Xilamulun metallogenic belt, NE China. *Resource Geology* **61**(3), 241–258.

**Zeng, Q.D., Liu, J.M., Chu, S.X., Wang, Y.B., Sun, Y., Duan, X.X., Zhou, L.L. 2012**. Mesozoic molybdenum deposits in the East Xingmeng orogenic belt, northeast China: characteristics and tectonic setting. *International Geology Review*, DOI:10.1080/00206814.2012.677498.

**Zhang, L.C., Wu, H.Y., Wan, B., Chen, Z.G. 2009**. Ages and geodynamic settings of Xilamulun Mo–Cu metallogenic belt in the northern part of the North China Craton. *Gondwana Research* **16**, 243–254.

**Zhao, Z.F., Zheng, Y.F., Wei, C.S., Wu, Y.B. 2004**. Zircon U–Pb age, element and oxygen isotope geochemistry of Mesozoic intermediate-felsic rocks in the Dabie Mountains. *Acta Petrologica Sinica* **20**(5), 1151–1174 (in Chinese with English abstract).

**Zhou, X.H., Zhang, G.H., Yang, J.H., Chen, W.J., Sun, M. 2001**. Sr–Nd–Pb isotope mapping of Late Mesozoic volcanic rocks across northern margin of North China Craton and implications to geodynamic processes. *Geochimica* **30**(1), 10–23 (in Chinese with English abstract).

**Zindler, A., Hart, S. 1986**. Chemical geodynamics. *Annual Review of Earth and Planetary Science* **14**, 493–571.

Scientific editing by Erdin Bozkurt

 